Transport in Porous Media **6**: 407–433, 1991.

Relative Permeabilities from Two- and Three-Dimensional Pore-Scale Network Modelling

MARTIN BLUNT and PETER KING
BP Research Centre, Chertsey Road, Sunbury-on-Thames, Middlesex. TW16 7LN, U.K.

(Received: 27 November 1989; revised: 12 July 1990)

Abstract. We present a computer study of two-phase flow in a porous medium. The porous medium is represented by an isotropic network of up to 80 000 randomly placed nodes connected by thin tubes. We then simulate two-fluid displacements in this network and are able to demonstrate the effects of viscous and capillary forces. We use the local average flow rates and pressures to calculate effective saturation dependent relative pemeabilities, fractional flows and capillary pressures. Using a radial Buckley–Leverett theory, the mean saturation profile can be inferred from the solution of the fractional flow equation, which is consistent with the computed saturation. We show that the relative permeability may be a function of both viscosity ratio and capillary number.

Key words. Network modelling, relative permeability, simulation, viscous fingering, capillary forces.

1. Introduction

Fluid displacements in porous media occur over a vast range of length scales. The fluids move through a disordered labyrinth of pore spaces which are only a few microns in diameter, and yet displacements in oil reservoirs are, typically, several kilometers in extent.

At the pore scale, the fluid flow is described by the Navier–Stokes equation. The boundary conditions at the interfaces between fluids and between a fluid and the solid rock matrix means that exact solutions are difficult to obtain for all but the simplest cases. Moreover, the exact nature of the contact between moving immiscible fluids is still not completely understood. Nevertheless it is possible to predict the fluid flow in several idealised pore geometries, such as through cylindrical or conical pipes.

On the scale of core samples, Darcy's law is an experimental relationship between flow rate and pressure gradient. A generalisation to two-phase flow is made by using saturation-dependent relative permeabilities and capillary pressures. In theory, it should be possible to demonstrate these macroscopic equations by averaging over the microscopic pore-scale processes. This approach has been attempted many times (Scheidegger, 1954; Miller and Miller, 1956; Whitaker, 1966, 1986; Poreh and Elata, 1966; Matheron, 1967; Lungren, 1972; Gray, 1975; Hassanizadeh and Gray, 1979; Levine and Cutheill, 1986; Rubenstein, 1986; Adler and Brenner, 1988; Pavonne, 1989). However, in order to obtain simple flow equations, approximations about the microscopic physics and the structure of the porous medium have to be made.

The goal of this work is to indicate how pore-scale processes lead to macroscopic displacements with definite averaged properties. We show the link between micron-scale physics and observable, centimeter-scale effects.

To determine how the microscopic pore-scale physics affects the overall macroscopic properties of the displacement, we simulate flow in a computer network model of a porous medium. The small-scale physics is precisely specified, and for networks containing many thousand pore spaces, we can find suitable averaged parameters to describe the macroscopic flow. Unlike an experimental system, we have complete control over the fluid viscosities and capillary forces. Also, we are able to compute saturations and pressures everywhere in the network with arbitrary accuracy.

We test whether or not fractional flows, capillary pressures and relative permeabilities are functions only of the local saturation. We also show the effect of the relative permeability on viscosity ratio and capillary number, or flow rate. This work identifies appropriate functions and variables for the description of two-phase flow.

2. The Simulation

Network models have been used before to study fluid displacements. Some of the first work was performed by Payatakes (1982). More recently, Koplik and Lasseter (1984), Chen and Koplik (1984), Chen and Wilkinson (1985, 1986) and Lenormand *et al.* (1984, 1985, 1986a, b, 1988, 1989) have simulated fluid flows in square grids of thin tubes of varying radius. Moreover, they were able to compare the numerical results with experimental patterns obtained from micromodels constructed from capillary tubes or etched networks. A porous medium is thus represented by a regular two-dimensional network of interconnected pore spaces. We have already described a network model on a hexagonal grid (King, 1987; Blunt and King, 1988). These simulations were in two dimensions and there was no capillary pressure.

Large displacements in models with regular grids are, however, anisotropic, displaying the symmetry of the underlying lattice, whereas real porous media are disordered. Moreover, all the work on large lattices only studied two-dimensional flows. As yet, there has been no consistent characterisation of the patterns produced in terms of conventional macroscopic parameters.

This work attempts to overcome all these shortcomings. We perform simulations in two- and three-dimensional isotropic networks and use Darcy's law and radial Buckley–Leverett theory to describe the displacement in terms of saturation-dependent fractional flows and capillary pressures.

2.1. GENERATING RANDOM NETWORKS

2.1.1. *Two Dimensions*

We have generated large topologically disordered, isotropic networks. To form a two-dimensional network, points are placed at random (called Poisson points) in a

circular region. The points are then connected to near-neighbours by nonintersecting bonds. The bonds form a triangulation of the region. We have chosen bonds so that the triangles are as near equilateral as possible. This is called a Delaunay triangulation (see, for instance, Ripley, 1981) (Figure 1). Essentially, the Delaunay triangulation is a consistent, straightforward way of connecting points to near-neighbours. In a two-dimensional Delaunay triangulation, each point is connected to, on average, six others, although the coordination number of a given point may vary from 3 to over 12. We have generated Delaunay triangulations containing up to 80 000 points. The methods used are described in greater detail elsewhere (Blunt *et al.*, to be published; Sever, 1986).

Delaunay networks have been considered previously as a representation of a random porous medium by Heiba *et al.* (1982). However, although they illustrated a Delaunay triangulation, they actually performed calculations of relative permeability on topologically simpler Bethe trees or regular networks.

In the model porous medium, the nodes of the network represent pore spaces of equal volume. The connections are thin tubes of an uncorrelated radius, r, chosen uniformly from the interval $[r_0(1-\lambda), r_0(1+\lambda)]$, where $1 \geqslant \lambda \geqslant 0$. We define l_0 as the average tube length and assume that $l_0 \gg r_0$.

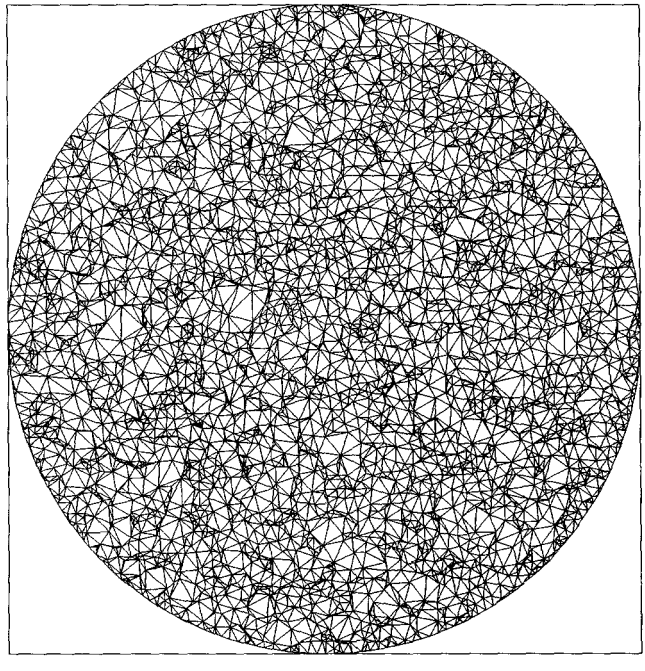

Fig. 1. A Delaunay triangulation of 4000 points in a circle. In the simulations a network with 80 000 points was used.

2.1.2. *Three Dimensions*

The three-dimensional analogue of the Delaunay triangulation above gives an average configuration number of over 14. The computer memory required to store all these connections would mean only comparatively small three-dimensional networks could be used.

Thus, we used an alternative lattice which is generated from a dual network, or Voronoi tessellation. This is formed from the Wigner–Seitz cells of each point, i.e. the territories nearer to each point than any other (Figure 2). An area is filled with polygons whose edges and vertices describe the network, a volume is filled with polyhedra.

For the two-dimensional Voronoi tessellation illustrated in Figure 2, each node has three connections. Equivalent three-dimensional networks in a spherical region have been generated, where every vertex or node has exactly four nearest neighbours. The disadvantage of this lattice is that the connectivity is fixed and so some of the topological disorder seen in real porous media is lacking. However, we are easily able to produce Voronoi networks containing up to 50 000 vertices.

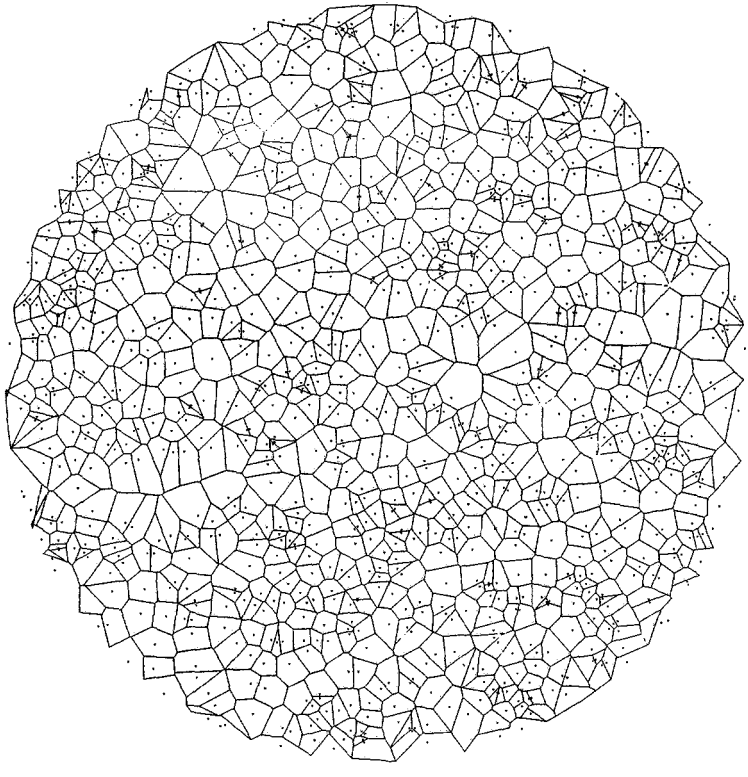

Fig. 2. A Voronoi tessellation of 500 points in a circle. Parts of the network which should lie outside the circle are placed around the circumference. The network contains approximately 1500 vertices each connected to three neighbours. Three-dimensional analogues with up to 50 000 vertices were generated.

The vertices of the Voronoi polyhedra represent the pore spaces and the edges between them are interconnecting tubes of variable radius. The radii are chosen in the same way as in two dimensions.

2.2. FLUID FLOW IN THE NETWORK

We model the flow through the networks using the following assumptions:

(a) All the fluid is considered to be contained in the pores or nodes, but all the pressure drops occur in the tubes between them.
(b) The tubes are totally filled with either invading or displaced fluid, but the pores may contain both fluids.
(c) The two fluids are immiscible. The invading fluid is nonwetting.
(d) The capillary pressure difference across an interface between the two fluids at the entrance of a tube is inversely proportional to the tube radius. The nodes are so wide that the capillary pressure drop in a node is neglected.
(e) There is Poiseuille flow down each tube.
(f) The fluids are incompressible.

2.2.1. *The Pressure Equation*

Poiseuille's law for the flow rate Q_{ij} between the tube connecting nodes i and j with no interface in the tube is

$$Q_{ij} = \frac{\pi(p_i - p_j) r_{ij}^4}{8 l_{ij} \mu} = g_{ij} \Delta p_{ij}, \tag{1}$$

where p is a nodal pressure, r_{ij} and l_{ij} are the radius and length, respectively, of the tube, and μ is the viscosity of the fluid in the tube. In a single node, the pressure of the injected and displaced phases are the same. This expression gives a flow rate which is proportional to the local pressure gradient and inversely proportional to the fluid viscosity.

If the fluids are incompressible then $\Sigma_j Q_{ij} = 0$. This enables us to solve for the pressure field p_i using successive over relaxation:

$$p_i = \beta \frac{\Sigma_j g_{ij} p_j}{\Sigma_j g_{ij}} + (1 - \beta) p_i, \tag{2}$$

where the sum over j accounts for all nodes connected to node i. The relaxation parameter β is set to 1.7.

2.2.2. *Updating the Saturation*

We use Equation (1) to update the volume of injected fluid in the nodes. In a time Δt, a nodal saturation $s_i(t)$ becomes

$$s_i(t + \Delta t) = s_i(t) + \Delta t \sum_j Q_{ij}$$

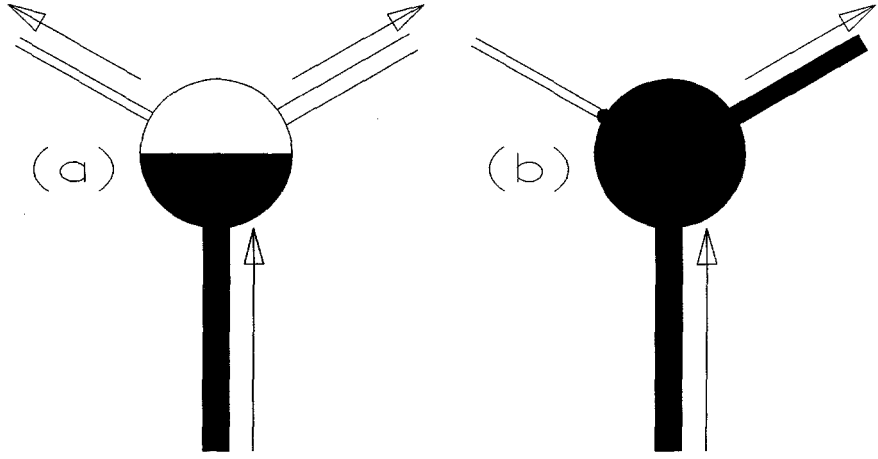

Fig. 3. Diagram showing the saturation update in a single node. (a) Injected (black) fluid is displacing clear fluid. Any pressure jump across the interface in a node is neglected. (b) The node is filled with injected fluid. A tube connected to this node may become full of invading fluid, or the interface may be frozen at the entrance of a tube by capillary pressure. Flow is most likely to be inhibited in narrow tubes.

where the sum only includes bonds connected to node i which contain invaded fluid. Δt is chosen so that only one node in every time step becomes completely filled.

When s_i does reach 1, then bonds connected to node i full of displaced fluid ('empty' bonds) may become full of invaded fluid. An empty bond of radius r_{ij} is filled with invaded fluid if

$$p_i \geqslant p_j + p_c, \tag{4}$$

where p_c represents the capillary pressure jump across the fluid interface in the tube. p_c is given by the Young–Laplace equation $p_c = -2\gamma \cos\theta / r_{ij}$. Notice that p_c is inversely proportional to the tube radius. γ is the interfacial tension and θ is the contact angle. We will consider the injection of a nonwetting fluid in this paper, with $\theta = 180°$ and, hence, $p_c = 2\gamma / r_{rij} \geqslant 0$. If $p_j + p_c > p_i \geqslant p_j$, then the interface is frozen by capillary pressure and no flow occurs across it until p_i increases, i.e. the conductivity, g_{ij} in Equation (1) is zero. This is illustrated in Figure 3.

In some nodes, s_i may decrease. If s_i reaches zero, a bond is filled with displaced fluid if $p_i \geqslant p_j$. Notice that if $\gamma = 0$, the displaced and invaded fluids are treated symmetrically.

Viscous forces control the fluid fluxes between nodes. The fluid in a tube only changes if the saturation in a node to which it is connected (at either end) rises to 1 or falls to 0.

2.2.3. *Boundary and Initial Conditions*

Initially, the network is full of displaced fluid. Nonwetting fluid is injected through a central node at a fixed rate. Fluid escapes through the outer boundary of the network, which is held at a constant pressure.

We have chosen to perform the simulations in circular and spherical networks for two reasons. Firstly, we wished the simulations to be unaffected by constraining boundaries, which for high flow rates may affect the overall pattern of the displacement, particularly in a channelled, square or cylindrical geometry. For instance, in a two-dimensional channel, it is known that at high flow rates, a single large finger develops, whereas in situations without a constraining boundary, a cascade of finger splitting is seen (Nittmann *et al.*, 1985; Chen and Wilkinson, 1985; Lenormand *et al.*, 1985, 1988). Secondly, in two dimensions, the averaged equations of flow with capillary pressure collapse to a simple scaling form (see Section 4), which would not occur for a square geometry. However, most previous work has been performed in rectilinear or cylindrical geometries, where relative permeabilities and capillary pressure are easier to interpret. On balance, a radial geometry is a good choice for investigating displacements at a high flow rate, but is less satisfactory for the discussion of capillary-dominated flows.

We inject fluid through a single node. At very low rates, it is occasionally found that the injection pressure needs to rise to force the fluid through the small number of tubes near the injector, and then the pressure falls again as the flow pathways are opened. This makes a small effect on the computed capillary pressure curves at low saturation, but does not alter the development of the displacement away from the centre.

The scheme is then as follows:

(a) Solve for the pressure p_i, using Equation (2).
(b) Calculate a time step Δt such that only one node is filled at a time.
(c) Update the saturations, using Equation (3).
(d) If the saturation in a node reaches 1 or 0, alter the nature of the fluids in the bonds connected to that node, as described above. The conductivities g_{ij} are recalculated from Equation (1), or set to zero if the fluid interface is frozen by capillary pressure.
(e) Repeat from step (a).

2.2.4. *Flow Parameters*

We simulate flow at a constant injection rate. The injection rate $Q_0 = \Sigma_j Q_{1j}$, where the subscript 1 labels the central injection node and the sum runs over all the tubes connected to the injector. The individual rates Q_{ij} are found from Equation (1). Before every saturation update, the injection pressure is altered so Q_0 remains constant and the rest of the pressure field is modified to ensure that $\Sigma_j Q_{ij} = 0$ everywhere.

We are now able to characterise the flow by the following dimensionless numbers:

(a) λ, which is a measure of the bond width disorder. The network is heterogeneous, since the individual bond conductivities g_{ij} vary widely. Firstly, the tube radii are chosen at random. A tube radius r is chosen uniformly from

the interval $[r_0(1-\lambda), r_0(1+\lambda)]$, where $1 \geqslant \lambda \geqslant 0$, as mentioned before. Secondly, the bond lengths are variable, about a mean l_0, which is not the case for a regular lattice.

(b) M, the ratio of displaced to injected fluid viscosities. $M = \mu_d/\mu_i$.

(c) N_c, a dimensionless capillary number, which is defined by: $N_c = Q_0 l_0 \mu_i / \pi \gamma r_0^3$.

N_c is chosen as above to represent a ratio of viscous to capillary pressure drops across a bond near the injection site. $N_c = 0$ gives capillary-dominated floods, while $N_c = \infty$ is viscous dominated. Increasing the flow rate Q_0 or decreasing γ will both increase the relative importance of viscous to capillary forces.

In a two-dimensional radial geometry, the viscous pressure gradient decreases as the inverse of radius from the injection node. Consequently, capillary forces become relatively more important at larger radii. For instance, in a two-dimensional displacement of 2000 filled sites, the flood has an overall radius of approximately 25 nodes. Thus if $N_c = 5$, the actual ratio of viscous to capillary forces at the advancing front is only about 5/25 or 0.2; viscous pressures dominate near the inlet, but capillary pressures control the pore-scale movement at large radius.

3. Discussion of Results

The simulations presented in this section have been performed on a two-dimensional network containing 80 000 nodes. This means that the network is approximately 350 nodes across. If typical distances between pore spaces in, for instance, a permeable sandstone range from 10 to 100 microns, then the network represents a sample a few centimetres in diameter. We will present some three-dimensional results in Section 4.

3.1. VISCOUS FINGERING

Figure 4 shows results for the case $N_c = \infty$, $\lambda = 0.5$. Capillary forces are neglected and we see viscous fingering patterns for a variety of adverse viscosity ratios from $M = 1$ to $M = \infty$.

In Figure 4(a), $M = 1$ and the interface between the fluids is marginally stable. The displacement has filled 20 000 nodes from a total of 80 000. The heterogeneity of the network causes small perturbations in the advancing front. This means that the relative permeability need not be an exact straight line, which would only be obtained from a completely smooth front. The invading fluid enters wide tubes first in preference to narrower ones. This means that occasionally small, low permeability blobs of displaced fluid are surrounded by the invading fluid. This is possible, even when we take the limit of large N_c. These blobs will eventually be swept out of the network, but they move very slowly, which will result in calculated relative permeabilities, which appear to have a residual saturation. This is not the case: the blobs are mobile, but flow at an almost imperceptable rate.

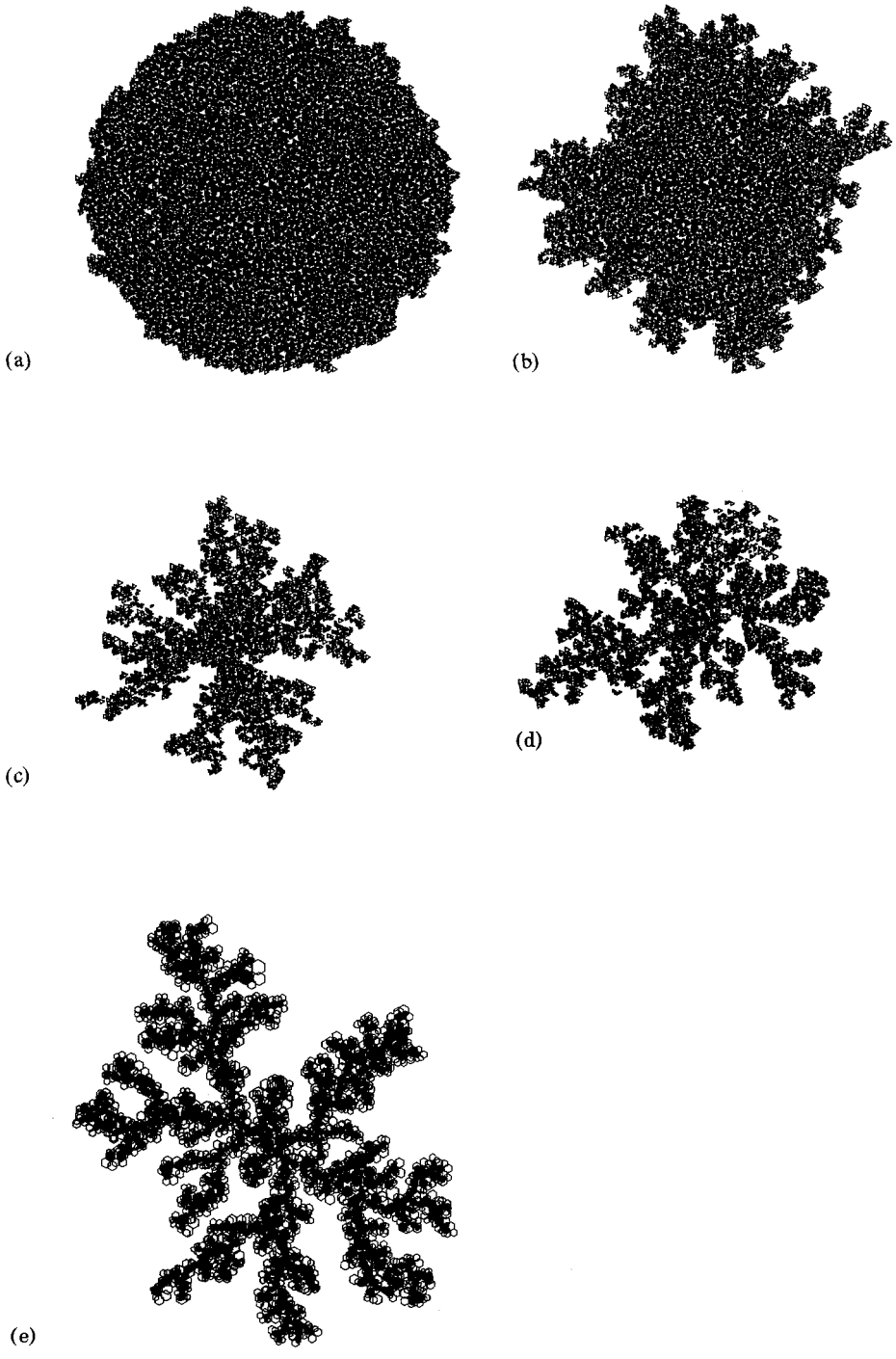

Fig. 4. Viscous fingering patterns for $N_c = \infty$, $\lambda = 0.5$. (a) $M = 1$. (b) $M = 10$. (c) $M = 100$. (d) $M = 1000$. (e) $M = \infty$. Open triangles or hexagons represent nodes which have yet to become completely filled.

When the viscosity ratio, M is greater than 1, the fluid interface is unstable and a fingered pattern develops. As M increases the fingering becomes more pronounced. The invading fluid, since it has a lower viscosity, moves more easily through the network than the fluid it displaces, and we see tip splitting and finger growth on all length scales. Although the saturation decreases sharply at the advancing tip of a single finger, the averaged radial saturation profile is smooth. The pattern for $M = \infty$ is extremely ramified and very thin fingers penetrate the network. In this case, the simulation is performed by assuming that there is no pressure drop in the invading fluid: all the pressure gradients are in the displaced fluid. The displacement in this case is similar to those observed experimentally by Måløy *et al.* (1985), which was also performed in a circular geometry, where a low viscosity fluid was injected at a high rate into a quasi-two-dimensional porous medium.

3.2. CAPILLARY DOMINATED DISPLACEMENTS

Figure 5 shows a simulation for an opposite case: $N_c = 0$, $\lambda = 0.5$. Here capillary forces are dominant. This process, called invasion percolation (Chandler *et al.*, 1982; Wilkinson and Willemsen, 1983), has been simulated directly. At the interface between the two fluids, the flow only proceeds along the widest available empty bond (as long as it does not connect to a region entirely surrounded by invading fluid), where the capillary pressure is lowest. All other bonds are frozen. The advance of the front is independent of M, as viscous forces may be neglected. Notice that we have loops enclosing pools of displaced fluid of many sizes.

Breakthrough occurs when the invading fluid first spans the system. Since the displacement is extremely ramified, this will occur at a very low overall saturation

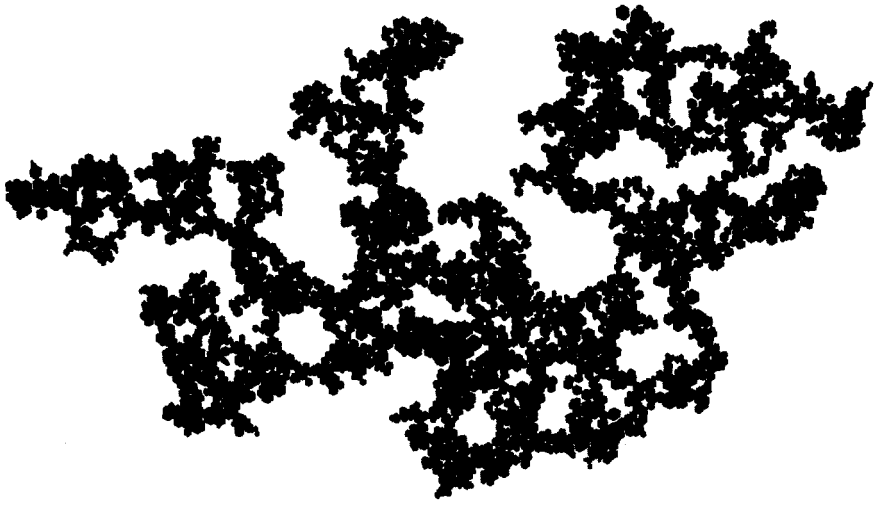

Fig. 5. Invasion percolation in a Delaunay triangulated lattice.

for large networks. The *terminal point* is defined when all the defending fluid is trapped in immobile blobs and the displacement ends. It has been demonstrated that, in two dimensions, the terminal point occurs at an infinitesimal increase in saturation after breakthrough in large systems (Wilkinson and Willemsen, 1983). This is because in two dimensions, it is not topologically possible to have intersecting continuous pathways of two phases. This means that the relative permeability is zero at all but saturations close to 0, and the capillary pressure curve is only defined near the origin. Clearly, this is fundamentally different from experimentally observed behaviour in three-dimensional rocks. In three dimensions, breakthrough also occurs at almost zero saturation, but both fluid phases may flow until the terminal point is reached at saturation values typically near 50%.

Figure 6 illustrates results when there are competing viscous and capillary forces. In the pictures, $M = 10$, $\lambda = 0.5$, and N_c is increased from 0 to 5. When $N_c = \infty$ (shown in Figure 4(b)) advance may occur at all points along the fluid boundary; on decreasing N_c more and more bonds at the fluid interface are frozen by capillary pressure, until, when $N_c = 0$ the flow is controlled entirely by the search for the easiest path of wide tubes through the network. This is demonstrated in Figure 7, which shows the number of filled tubes as a function of radius at breakthrough: when $N_c = \infty$ wide and thin tubes are filled with almost equal probability, except at very low saturation; when $N_c = 0$, no tubes thinner than a percolation threshold are filled at all.

Lenormand *et al.* (1985, 1988) have already investigated two-phase displacements in square networks of capillary tubes, both numerically and experimentally, as a function of capillary number. When N_c is very low and a nonwetting fluid is injected, the patterns are similar to results from an invasion percolation model (Lenormand and Zarcone, 1985). This has also been confirmed experimentally by Stokes *et al.* (1986). Moreover, Lenormand observed similar patterns to ours for large N_c and $M > 1000$ and $M = 1$ (Lenormand *et al.*, 1988), with a cross-over from capillary to viscous dominated flows at intermediate capillary numbers. These studies confirm that our simulations give valid results in two dimensions in the limit of both very high and very low flow rates. We have extended the model to three dimensions and we look at random networks, which have not been studied before. Furthermore, we compute macroscopic dynamic parameters, such as relative permeability and fractional flow, which were not investigated by Lenormand *et al.*

In a real oil reservoir, capillary forces are likely to dominate at the pore scale, with a typical viscous pressure drop along a single tube, Δp_v, one hundred to several thousand times smaller than the capillary pressure drop across a fluid interface. However, over large distances or near wells, the viscous pressure drop will normally exceed the capillary force. In a radial flood, Δp_v decreases with distance from the injection node: we see viscous floods near the centre of the network with capillary forces becoming more important on the pore scale at large radii.

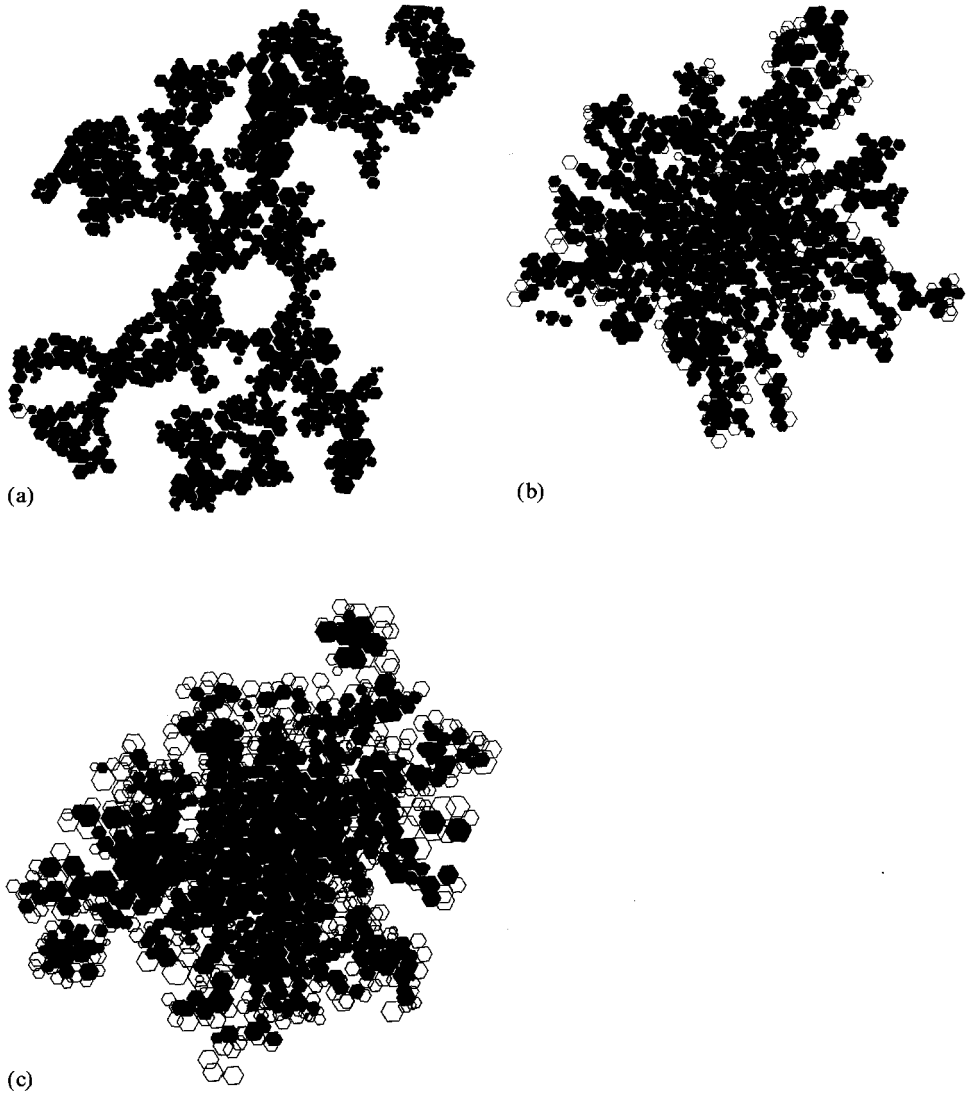

Fig. 6. Displacements for $M = 10$, $\lambda = 0.5$ each containing approximately 1500 nodes. (a) $N_c = 0$. (b) $N_c = 0.5$. (c) $N_c = 5$. Notice that the number of partially filled sites (shown by open hexagons) increases with N_c. For $N_c \approx \infty$ (Figure 4) the displacements are completely surrounded by partially filled nodes. The exact microstructure of the network is different in all these cases.

Hence, the pore-scale motion is capillary dominated, while viscous forces determine the overall profile of large displacements. Thus, the macroscopic nature of fingering is usefully determined by investigating viscous dominated flows. Also, it is interesting to probe the cross-over regime where both viscous and capillary forces are important, which is the situation found typically in centimetre-scale core floods, where we might expect to see values of N_c in the range 0.1 to 10.

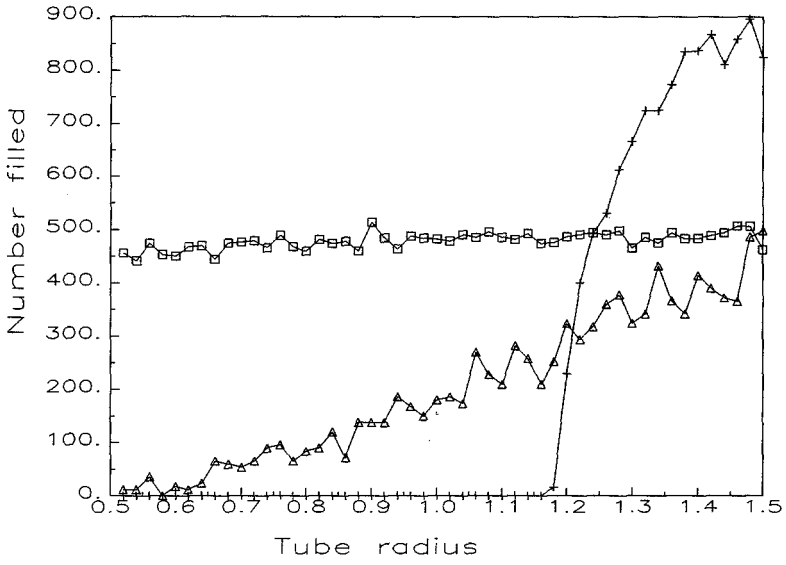

Fig. 7. Histogram of the number of filled tubes against tube radius for $M = 10$, $\lambda = 0.5$. Crosses $N_c = 0$; triangles $N_c = 0.5$; squares $N_c = \infty$. Notice that for $N_c = 0$ no tubes thinner than a percolation threshold are filled.

4. A Conventional Description

Our model describes pore-scale flow. However, in simulations of reservoir flows, the microscopic physics in large grid blocks is represented by simple averaged parameters. A justification for this approach will be provided by this work.

4.1. RADIAL BUCKLEY–LEVERETT THEORY

In this section, we will assume that the conventional averaged description of flow in a porous medium can correctly describe the behaviour of our simulated displacements. A short mathematical analysis leads to a prediction for the development of the angularly averaged saturation profile in two dimensions. We test this prediction against the computed results. We also demonstrate how the fractional flow and relative permeability depend on viscosity ratio and capillary number.

In Section 2, we specified the micro-scale physics of flow. However, this description is inappropriate if we wished to write down equations for the flow on scales averaged over many individual pores.

Conventionally, we assume a two-phase Darcy law in a porous medium (Muskat and Meres, 1936; Peaceman, 1977):

$$\mathbf{q}_d = -K\frac{k_{rd}(s)}{\mu_d}\nabla p_d, \tag{5}$$

$$\mathbf{q}_i = -K\frac{k_{ri}(s)}{\mu_i}\nabla p_i, \tag{6}$$

where the subscripts i and d refer to the invading and displaced fluids, respectively, q is a fluid flux per unit area, and K is the absolute permeability of the medium. The Poiseuille flow at the pore scale, Equation (1), should ensure that the fluid fluxes are proportional to a local pressure gradient and inversely proportional to the viscosity.

The relative permeabilities k_{ri} and k_{rd} are generally assumed to be functions of the saturation of injected fluid only. This saturation ($s = s_i$), where $s_i + s_d = 1$, is a mean value taken over several nodes. The relative permeability takes into account the effect of averaging over a representative volume containing many pores.

The difference between p_i and p_d is given by a saturation dependent capillary pressure, i.e. $p_i - p_d = P_c(s)$ (Leverett, 1941). There is no rigorous justification for these simplifications: k_r and P_c may also depend systematically on the degree of development of the displacement, or be largely independent of the average saturation and be controlled by pore-scale properties. Marle (1981) has demonstrated that the relative permeability may depend in theory on the dimensionless parameters M and N_c as well as the wetting properties of the rock and fluids. Furthermore, k_r may not be simply a function of local saturation s only, but may depend also on derivatives of s, such as $\mathrm{d}s/\mathrm{d}x$, and $\mathrm{d}^2s/\mathrm{d}x^2$.

The representative volume over which the saturation is averaged must be greater than the volume of an individual pore, yet much smaller than the overall size of the system under consideration. For a reliable determination of relative permeability, it is necessary that we average over a region which genuinely represents a macroscopic sample. Rather than postulate what the minimum representative volume should be, we computed the relative permeabilities in our numerical model using annuli of different widths. The networks we used were approximately 350 nodes across. When the annulus was less than 4 or 5 nodes wide, the results became increasingly noisy, although distributed about the values obtained when a larger sampling volume was chosen. When the average was taken over more than 50 nodes, there was a significant shift in the calculated relative permeabilities, since the volume element then encompassed significant changes in the overall saturation and pressure profiles. This shift was more marked when the saturation profile was sharp. The width of the averaging region must be smaller than any macroscopic length, such as the width of the fluid front and larger than any microscopic length, such as a pore diameter. In all the results we present later, we will average s in regions about 5 nodes wide, which contain approximately 2000 nodes each. This gives just a sufficient division of length scales to produce reliable results, which are insensitive to small changes in the averaging volume, regardless of capillary number.

With only viscous forces, Poiseuille flow occurs through all connections in the network. If the saturations and pressures are averaged in a small region of space in which we assume there is no fingering, then the relative permeabilities will have a simple, linear form: $k_{ri} = s_i$ and $k_{rd} = s_d$ (Dullien, 1979). Capillary forces, which cause the advance in some tubes to be frozen, will give relative permeabilities with a nonlinear dependence on saturation.

However, the pressure field and saturation profiles are very complicated for

$M > 1$, even for viscous flows, since we see an unstable, fingered front. In the analysis below, we will attempt a description where the pressures and saturations in Equations (5) and (6) are considered to be averaged over a thin annular region at a fixed distance, r from the injection node. Then the relative permeability k_r accounts not only for capillary forces, but also the averaged properties of the fingered displacement, and so may be nonlinear even for purely viscous floods.

Firstly we assume that Equations (5) and (6) are valid for angularly averaged pressures, saturations and fluxes. This means that they are valid if we substitute

$$p(r, t) = \frac{1}{2\pi} \int_0^{2\pi} p(r, t, \theta)\, \mathrm{d}\theta,$$

$$s(r, t) = \frac{1}{2\pi} \int_0^{2\pi} s(r, t, \theta)\, \mathrm{d}\theta$$

and

$$q(r, t) = \frac{1}{2\pi} \int_0^{2\pi} q(r, t, \theta)\, \mathrm{d}\theta.$$

Our second set of equations are those of fluid conservation with no source terms:

$$\frac{\partial s_i(r, t)}{\partial t} + \nabla \cdot \mathbf{q}_i(r, t) = 0 \tag{7}$$

and

$$\frac{\partial s_d(r, t)}{\partial t} + \nabla \cdot \mathbf{q}_d(r, t) = 0, \tag{8}$$

where we have assumed a unit porosity.

We add Equation (7) to Equation (8) to obtain a simple expression for the total flux, $\mathbf{q}_t = \mathbf{q}_i + \mathbf{q}_d$:

$$\nabla \cdot \mathbf{q}_t = 0. \tag{9}$$

In a two-dimensional radial geometry, averaging the angular dependence in the flow, $\mathbf{q}_t$ is directed in a radial direction and has the form

$$q_t = \frac{Q_0}{2\pi r}, \tag{10}$$

where Q_0 is the (fixed) injection rate, $\int_0^1 2\pi r s(r, t)\, \mathrm{d}r = Q_0 t$.

Equation (5) is added to Equation (6) to obtain

$$q_t = \frac{Q_0}{2\pi r} = -K[(\lambda_d(s) + \lambda_i(s))\, \nabla p_i - \lambda_d(s)\, \nabla P_c(s)], \tag{11}$$

where the fluid mobilities, λ are k_r/μ and p_d has been written as $p_i - P_c(s)$.

We use Equation (11) to find ∇p_i in terms of q_t and ∇P_c and then substitute q_i into Equation (7) using Equation (6):

$$\frac{\partial s}{\partial t} + \nabla \cdot \left[\frac{\lambda_i(s) Q_0}{2\pi(\lambda_d(s) + \lambda_i(s))r} - K \frac{\lambda_i(s)\lambda_d(s)}{\lambda_d(s) + \lambda_i(s)} \nabla P_c(s) \right] = 0. \tag{12}$$

This equation for fluid conservation may be written more simply in terms of a fractional mobility or flow: $F(s) = \lambda_i(s)/(\lambda_d(s) + \lambda_i(s))$:

$$\frac{\partial s}{\partial t} + \nabla \cdot \left[F(s) \left(\frac{Q_0}{2\pi r} - K\lambda_d(s) \nabla P_c(s) \right) \right] = 0 \tag{13}$$

from which we obtain

$$\frac{\partial s(r, t)}{\partial t} + \frac{1}{r} \frac{\partial}{\partial r} \left[F(s) \left(\frac{Q_0}{2\pi r} - Kr\lambda_d(s) \frac{\partial P_c(s)}{\partial r} \right) \right] = 0, \tag{14}$$

since the operator $\nabla \cdot$ is $1/r\partial(r)/\partial r$ in radial coordinates. Equation (14) may be written simply in terms of a single variable $v = \pi^{1/2} r/(Q_0 t)^{1/2}$ to obtain (after a little algebra)

$$\frac{\mathrm{d}s(v)}{\mathrm{d}v} \left\{ v^2 - \frac{\mathrm{d}}{\mathrm{d}s} \left[F(s) \left(1 - \frac{2\pi v K \lambda_d(s)}{Q_0} \frac{\mathrm{d}s}{\mathrm{d}v} \frac{\mathrm{d}P_c}{\mathrm{d}s} \right) \right] \right\} = 0 \tag{15}$$

and, thus, a nontrivial solution is obtained when

$$v^2 = \frac{\mathrm{d}}{\mathrm{d}s} \left[F(s) \left(1 - \frac{2\pi v K \lambda_d(s)}{Q_0} \frac{\mathrm{d}s}{\mathrm{d}v} \frac{\mathrm{d}P_c}{\mathrm{d}s} \right) \right]. \tag{16}$$

For a general $P_c(s)$, Equation (16) does not, unfortunately, have an analytic solution, although it may be obtained easily by numerical integration. However, it can be seen that the saturation profile is a function of only one variable, v, and hence profiles taken at different times may be scaled on to each other. For floods with nonzero P_c this is only possible because we have a radial geometry. For $P_c = 0$, Equation (16) reduces to a radial Buckley–Leverett problem, whose solution is $s(v)$ where $\mathrm{d}F/\mathrm{d}s = v^2$.

4.2. FRACTIONAL FLOWS

The analysis above has shown that mean saturation profiles taken at different times can be scaled on to the same curve, and that the fractional flow is a function only of saturation. We need to test this directly. For a variety of two-dimensional floods with different M and $N_c = \infty$, mean saturation profiles and fractional flows have been calculated at up to five different times. The network is divided into 40 annular sections. Within each annulus, the mean saturation of invaded fluid is calculated as well as the fraction of the total flux across each annulus carried by the invading fluid: in the absence of capillary pressure, this is the fractional flow $F(s)$. That this fractional flow is a unique function of the mean saturation is the central assumption of our analysis.

Example results are shown for $\lambda = 0.5$, $M = 10$, and $N_c = \infty$. Figure 8 shows the mean saturation profiles at different times successfully scaled on to a single curve; figure 9 shows indeed that $F(s)$ does not appear to depend only on s and not independently on time or radius for given model parameters. Moreover, we can use $s(v)$ to calculate $F(s)$, since $\mathrm{d}F/\mathrm{d}s = v^2(s)$, then $F(s) = \int_0^s v^2(s)\,\mathrm{d}s$. This is shown in Figure 9: both direct and inferred fractional flow agree to within numerical error. Notice that the fingered front is wide: the saturation profile does not develop a shock. This means that $F(s)$ does not have a point of inflexion.

Fractional flow curves for various M with $N_c = \infty$ and $\lambda = 0.5$ are illustrated in Figure 10. Increasing M gives a more fingered front and lower overall recovery. For $M = 1$, the fractional flow (and also the relative permeability shown later) is not exactly linear because of the fine scale heterogeneity of the network. Also, as discussed earlier, there is strictly no residual saturation when $N_c = \infty$, although the small trapped blobs of displaced fluid move very slowly.

Saturation profiles for $M = 10$, $\lambda = 0.5$ and $N_c = 0.5$ are shown in Figure 11, scaled onto the same curve. Notice that s appears to be a function of only one variable, v. Viscous fingering is supressed on increasing the capillary pressure, but pools of displaced fluid become enclosed by the invader for low N_c, which causes the overall fraction of displaced fluid swept out to decrease. Overall, the capillary pressure has a diffusive effect on the flow: Figure 12 shows that the profiles are smeared out for low N_c.

In all the examples, the saturation profiles do scale onto the same curve and the fractional flow is a function only of saturation for fixed M and N_c.

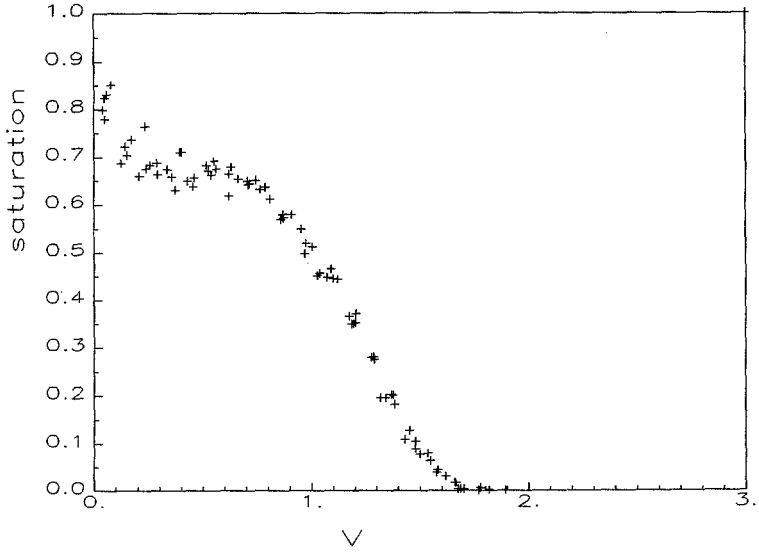

Fig. 8. The mean saturation profile s for $M = 10$, $\lambda = 0.5$, and $N_c = \infty$. The results of two simulations each taken at five equally spaced intervals during the flood have been scaled on to the same curve.

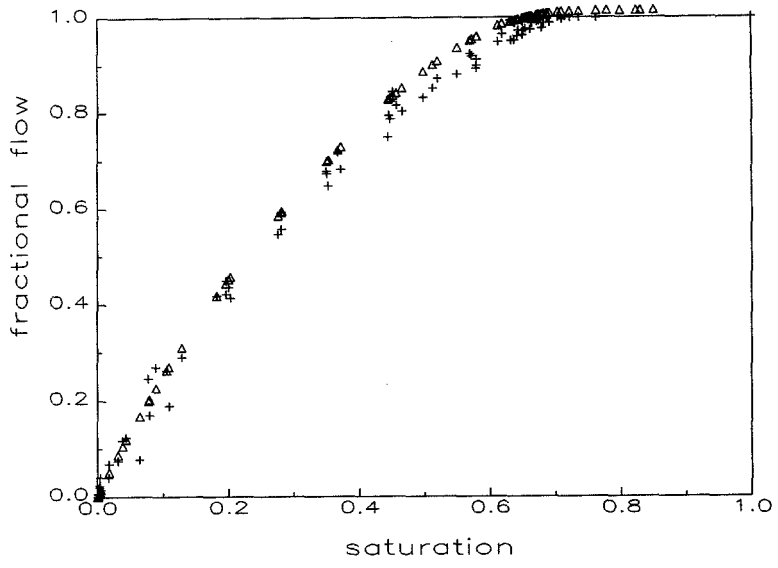

Fig. 9. The fractional flow curve $F(s)$ for $M = 10$, $\lambda = 0.5$, and $N_c = \infty$. F has been measured at five times during the growth for two different simulations. Crosses, direct measurement; triangles, calculated from the mean saturation profile.

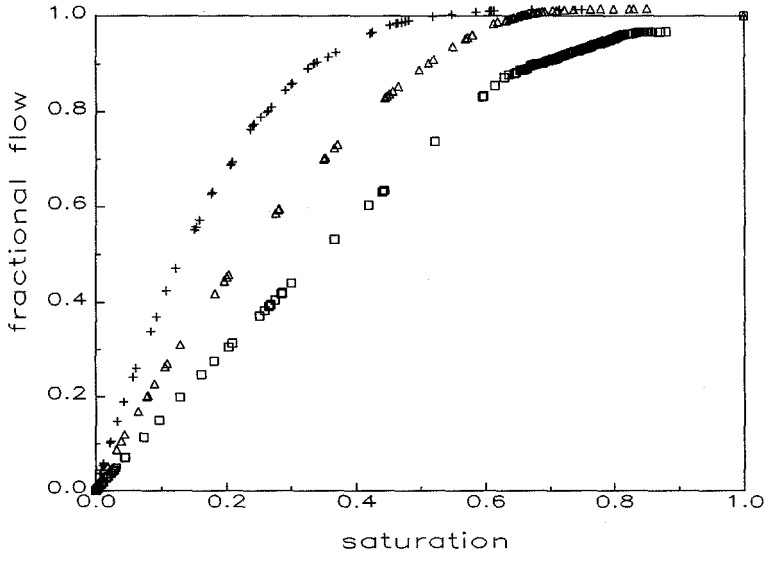

Fig. 10. Fractional flow curves calculated from mean saturation profiles for $N_c = \infty$ and $\lambda = 0.5$. Crosses $M = 100$; triangles $M = 10$; squares $M = 1$.

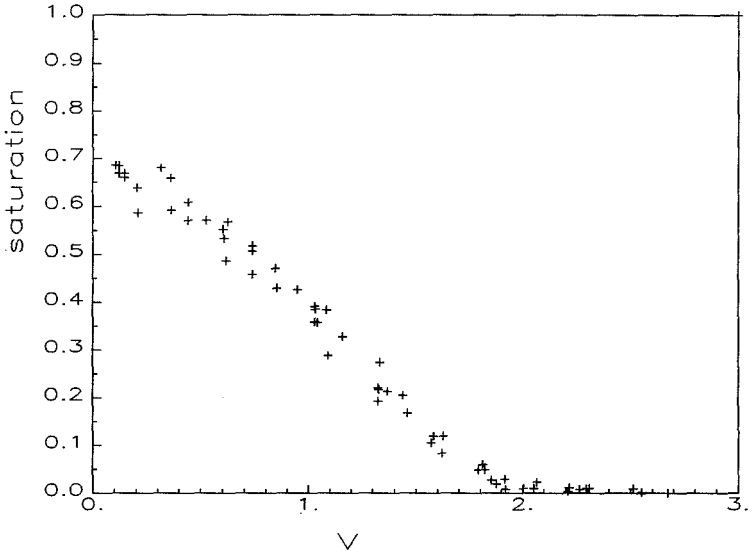

Fig. 11. Saturation profiles as in Figure 8 for $M = 10$, $\lambda = 0.5$, and $N_c = 0.5$.

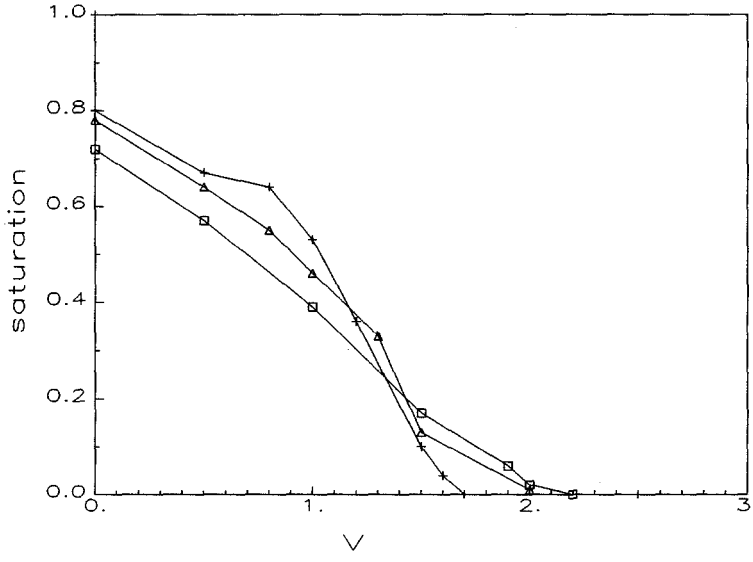

Fig. 12. Averaged saturation profiles for $M = 10$ and $\lambda = 0.5$. Crosses $N_c = \infty$; triangles $N_c = 5$; squares $N_c = 0.5$.

4.3. CAPILLARY PRESSURE CURVES

For finite interfacial tension γ, there is a pressure jump across the fluid interface: in an averaged description of the flow, this leads to an effective capillary pressure P_c, which we hypothesise to be a function of mean saturation s only. $P_c(s)$ is the difference between the pressures of invading and displaced fluids. This has been

computed at various stages during the growth in the different annuli dividing the network. Example curves in three dimensions for $M = 1$, $\lambda = 0.5$, and $N_c = 0$ and 0.5 are shown in Figure 13. The results in two dimensions are much poorer and are not presented here, since, as we discussed in Section 3.2, P_c is only well defined for saturations near zero for very low flow rates, which is clearly different from the behaviour of real three-dimensional systems.

P_c is measured in units of $2\gamma/r_0$. For $\lambda = 0.5$, the tube radii vary from $0.5r_0$ to $1.5r_0$ and so the maximum and minimum interfacial pressures in a single tube are $2 \times 2\gamma/r_0$ and $1/1.5 \times 2\gamma/r_0$, respectively. The shape of $P_c(s)$ for $N_c = 0$ is similar to capillary pressure curves obtained from mercury injection into rock samples (Dullien, 1979). The variation in capillary pressure is smaller than observed in most experimental systems, since our simulated radius distribution is narrower than in real rocks. Notice also that P_c rises steeply when only 36% of the nodes are filled: the remainder of the nodes are trapped in immobile ganglia surrounded by the injected fluid.

For $N_c = 0.5$, the capillary pressure is higher at low saturations, although there is no significant change in residual saturation (this is only seen at higher N_c). At low flow rates, narrow tubes are only filled by injected fluid when s is high, whereas at high rates, small tubes may also be accessed, because of the local effect of viscous forces. The comparative importance of capillary to viscous forces is measured by N_c. Thus, although $P_c(s)$ increases slightly with rate, relatively, the effect of capillary forces on displacement diminishes as N_c increases.

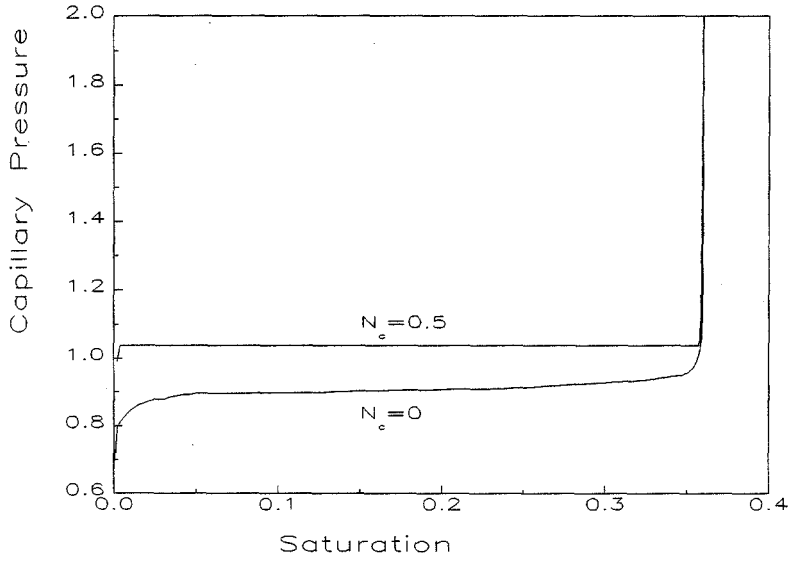

Figure 13. Averaged capillary pressure curves in three dimensions for $M = 1$ and $\lambda = 0.5$ and $N_c = 0$ and $N_c = 0.5$. The capillary pressure is measured in units of $2\gamma/r_0$, where γ is the interfacial tension and r_0 is a mean bond radius.

At a microscopic level, the functions F and P_c are meaningless, but we have demonstrated that the averaged properties of pore-scale flow may be described in terms of parameters which depend on the local saturation, and of course the properties of the network and the fluids, but not explicitly on time or radius.

4.4. RELATIVE PERMEABILITY

The fractional flow is the most natural function to describe the development of the saturation profile. However, this does not give us directly a relationship between the fluid flux and an averaged pressure gradient. If we wished to describe the flow in a very large network, we could model the fluid flow by the macroscopic Darcy's law, Equations (5) and (6), with numerically or experimentally determined relative permeabilities, k_{ri} and k_{rd}. It is these functions which account for the microscopic physics and which enable the complexity of pore-scale flow to be replaced by averaged macroscopic parameters.

We find the relative permeabilities directly in our simulation. We calculate the differences in mean pressure in the invading and displaced fluids, Δp_i and Δp_d, respectively, across the 40 annular sections dividing the network. The mean saturation in the annuli and the fluxes of invading and displaced fluids across them are also calculated. From these quantities we may calculate relative permeabilities using Equations (5) and (6):

$$k_{rd}(s) = \frac{q_d \mu_d x_0}{K \Delta p_d}, \tag{17}$$

$$k_{ri}(s) = \frac{q_i \mu_i x_0}{K \Delta p_i}, \tag{18}$$

where x_0 is the width of each annulus. The absolute permeability, K, is defined such that $k_{rd}(s = 0) = 1$, i.e. K is the permeability of the medium in single-phase flow. Notice that we assume that the viscosities μ have the same values as in single-phase flow. This is different from the interpretation in miscible flow, where it is assumed that $k_{ri} = s$ and so $\mu(s)$ is calculated to obey Equations (17) and (18). For immiscible flow, this means that the relative permeabilities are likely to be nonlinear, because of viscous fingering, even when $N_c = \infty$, if $M \geqslant 1$.

Example curves are shown in Figure 14 for $M = 1$ and $N_c = \infty$ in two dimensions. The quality of the data is not as good as for the fractional flow curves, since we have needed to use computed pressure gradients. The heterogeneity of the network initiates some fingering and the invading nonwetting fluid traps a small fraction of slowly moving displaced fluid. Hence, the relative permeability departs slightly from the linear form expected in smooth viscous flows in a homogeneous medium.

Three-dimensional results for $M = 1$ and $N_c = \infty$ and $N_c = 0$ are shown in Figure 15.

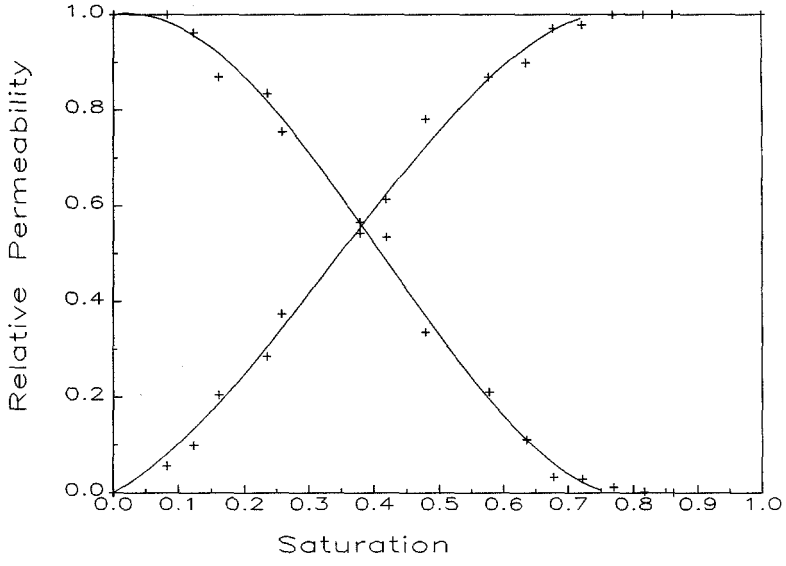

Fig. 14. Relative permeability curves for $M = 1$ and $N_c = \infty$ in two dimensions as a function of saturation. By definition, the invading fluid curve has $k_{ri}(0) = 0$ and the displaced fluid has $k_{rd}(0) = 1$. The curves are polynomial fits to the computed points.

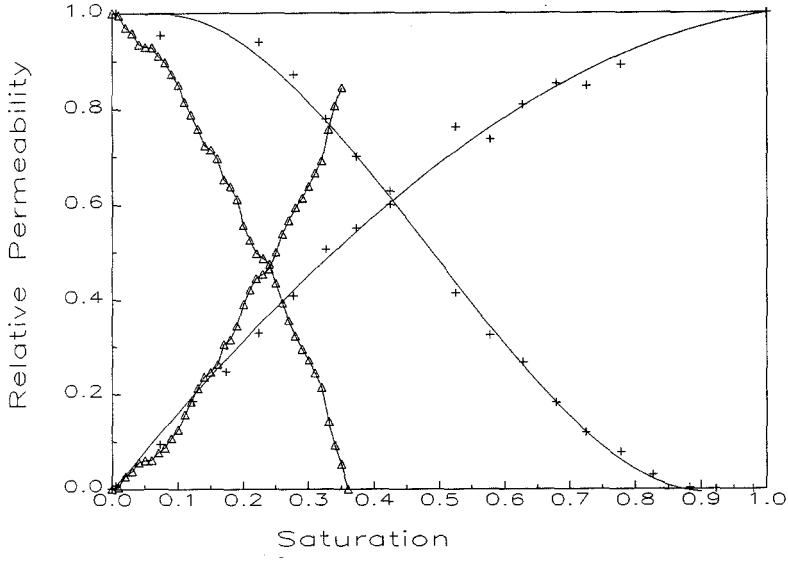

Fig. 15. Relative permeability curves in three dimensions for $M = 1$. Crosses, $N_c = \infty$; triangles, $N_c = 0$.

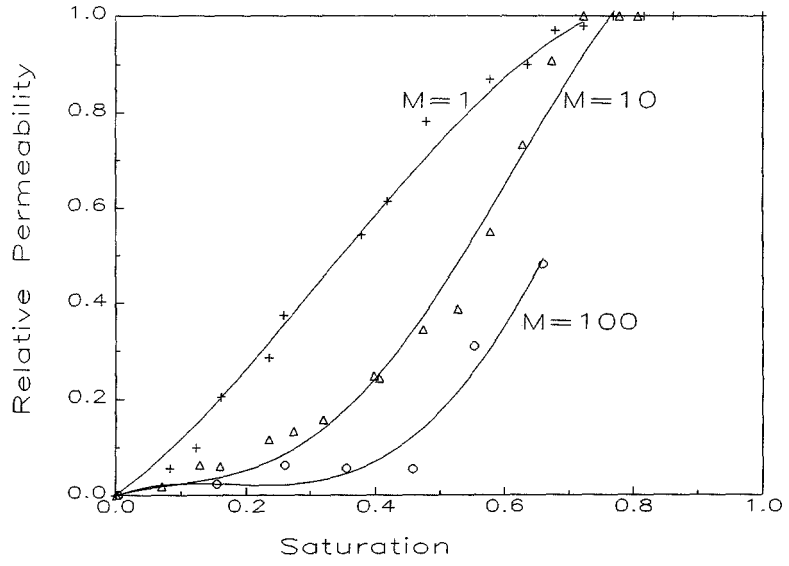

Fig. 16. Two-dimensional relative permeability curves for $N_c = \infty$ and for viscosity ratios, M, as shown. For clarity only the invading fluid curve is plotted.

Figure 16 shows the invading fluid relative permeability for two-dimensional viscous floods at different viscosity ratios. By averaging the fluxes, saturations and pressures over an annular region, we have accounted for fingering in the relative permeability, which as a consequence is a function of M. The nonlinearity of the curves is most marked for large M, indicating that, on the pore scale, the displacement is very unstable and highly fingered.

At low flow rates, experimental relative permeabilities are insensitive to viscosity ratio (Dullien, 1979), but at higher rates, which are simulated here, k_r is known to change (Odeh, 1959).

4.4.1. *Effect of Capillary Number*

At very high rates, flow can proceed through all parts of the network, including the very small tubes. As N_c decreases, flow is blocked in some places due to capillary forces. This will tend to decrease the relative permeability of both injected and displaced fluids. However, as we demonstrated in Figure 7, at low rates, the injected fluid moves through only the widest channels, which alone has the effect of increasing its permeability relative to the displaced fluid. Thus, at a given saturation, k_{rd} must decrease with decreasing rate, while k_{ri} may either increase or decrease. In two dimensions, the blocking of flow channels is the more significant effect, and when $N_c = 0$, the relative permeabilities are almost zero for nonzero saturations (see Section 3.2).

Figure 17 is the relative permeability for $M = 1$ and $N_c = 0.5$ in two dimensions.

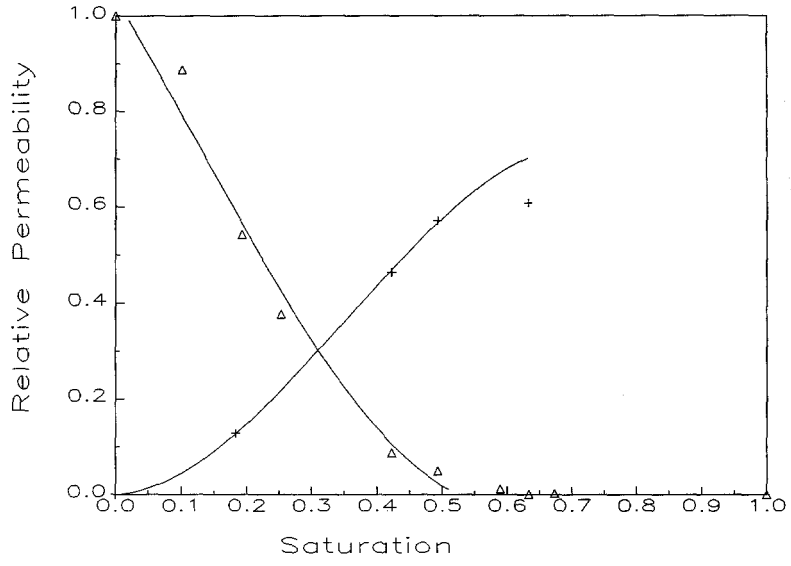

Fig. 17. Relative permeability curves for $M = 1$ and $N_c = 0.5$ in two dimensions.

The fluid interface is marginally stable to viscous fingering at unit viscosity ratio. However, capillary pressure inhibits the flow through narrow tubes, which causes a sharp front to smear out and increases the tendency for displaced fluid to be trapped. If Figure 17 is compared with Figure 14, it also is evident that the apparent permeability of the medium is decreased when the capillary pressure is increased. Freezing the fluid interface at narrow throats increases the resistance to flow.

Figure 18 shows the relative permeability for $M = 10$ and for two different capillary numbers. For $N_c = 5$, the curves are similar to those obtained for $N_c = \infty$ in Figure 14. However, for $N_c = 0.5$, we again see that the relative permeability curve is lower than for a purely viscous displacement.

In three dimensions, the blocking of channels is less significant at higher saturations, where the injected fluid finds a permeable pathway through the medium, bypassing any narrow tubes. This is demonstrated in Figure 15, which shows relative permeabilities for $N_c = 0$ and $N_c = \infty$. $k_{rd} = 0$ for $N_c = 0$ when only 36% of the nodes are filled. This indicates a very high residual saturation of 64%. The coordination number of the Voronoi lattice is only four, which makes it easy for the displaced phase to be trapped. In real systems, the effective coordination number is likely to be higher, giving a lower residual saturation.

The relative permeability is a function of capillary number for intermediate flow rates. It is, however, often assumed that the relative permeability is insensitive to N_c (overall flow rate or capillary pressure). When N_c is small this has been confirmed by many experiments, see, for instance, Amaefule and Handy (1982). However, Bardon and Longeron (1980) studied the gas relative permeability in a Fontainbleau sandstone as the interfacial tension γ was varied from 0.04 to 0.001 mM/m.

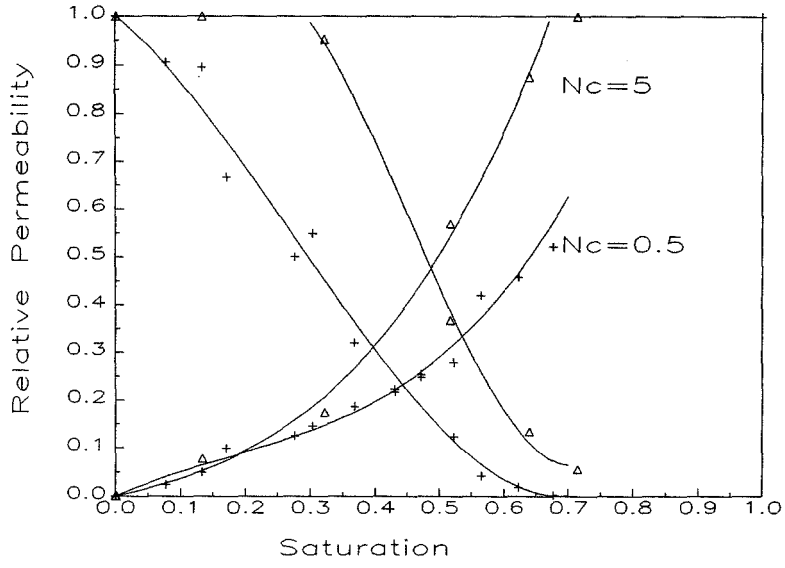

Fig. 18. Two-dimensional relative permeability curves for $M = 10$ and for the capillary numbers N_c shown.

Lowering γ effectively increases the capillary number. At the lowest interfacial tension, the relative permeabilities are almost exactly linear, but become increasingly curved as γ is increased. qualitatively, the results are similar to Figure 15, which shows three-dimensional relative permeabilities at very high and very low flow rates, except that the residual saturations are lower in the experiment. Quantitative comparisons are, unfortunately, not possible without some knowledge of the microscopic rock structure.

These relative permeabilities have been obtained in a macroscopically radial flow, where, at the pore scale, the local ratio of viscous to capillary forces decreases with radius from the injection site. However, the explicit radial dependence of the flux has been accounted for by Equation (10), leaving permeabilities which are functions of saturation only. A change in the global value of N_c alters the relative importance of viscous to capillary forces everywhere in the network.

5. Conclusions

We have used a network model of flow in porous media to study the effect of viscosity ratio and capillary pressure on pore-scale displacements in both two and three dimensions. With this model, we are able to show how the microscopic physics of flow affect averaged properties on the centimetre scale. We can indicate the appropriate functions necessary for a consistent and accurate description of the displacements and the parameters on which they depend.

In brief we may make the following conclusions:

(a) The mean saturation profiles are consistent with a Buckley–Leverett theory. This enables the floods to be described in terms of empirical parameters.
(b) For a displacement with a fixed viscosity ratio and capillary number, the fractional flow and relative permeability are functions of the local saturation only.
(c) The relative permeabilities have been shown to be functions of both capillary number at intermediate flow rate and viscosity ratios greater than unity.

We have proposed a conventional description in terms of saturations and pressures averaged over several pore volumes. This approach has been verified for floods in a radial geometry, where profiles at different times can be scaled onto a single curve. We have been able to compute effective relative permeabilities, fractional flows, and capillary pressures.

More detailed work and development should involve comparison of this model with results from experiment and conventional simulation.

In particular, the remaining problems and suggestions for more study include:

(a) The microscopic physics of fluid flow in porous media is still not completely understood, especially for invasion by a wetting fluid, which has not been studied here. Experimental and theoretical work could suggest simple yet realistic rules for modelling all types of displacement.
(b) More three-dimensional simulations could be performed. In particular, simulations in a cylindrical geometry could be performed.
(c) The effect of matrix heterogeneity on the flow has yet to be investigated.
(d) A direct comparison of experimental bead pack or network displacements with this model could be made.

Experimental work on micromodels of porous media can be used to determine the rules and equations necessary for a pore-scale description of immiscible displacement. This microscopic physics can be input into our numerical model, which is sufficiently large enough that quantitative computations of macroscopic effects can be made. We can then determine the correct averaged functions to describe the progress of the flow, the results of which can again be confirmed against core-scale experiments, which alone are unable to probe microscopic effects. The goal is to use this model as a tool for gaining a predictive understanding of flow in porous media from the micron to the centimetre scale.

Acknowledgements

We thank British Petroleum plc for permission to publish this paper. We should like to thank Dr R. C. Ball for useful discussions. We are also particularily grateful to Drs J. J. Barley and P. K. Sweby for providing us with programs for generating Voronoi meshes.

References

Adler, P. M. and Brenner, H., 1988, *Ann. Rev. Fluid Mech.* **20**, 35.
Amaefule, J. O. and Handy, L. L., 1982, *SPEJ* **22**, 371.
Bardon, C. and Longeron, D., 1980, *SPEJ* **20**, 391.
Blunt, M. J. and King, P. R., 1988, *Phys. Rev. A* **37**, 3935.
Blunt, M. J., King, P. R., Goshawk, J. A., and Ball, R. C. (to be published).
Chen, J-D., 1986, *J. Coll. Int. Sci.* **110**, 488.
Chen, J-D. and Koplik, J., 1985, *J. Coll. Int. Sci.* **108**, 304.
Chen, J-D. and Wilkinson, D., 1985, *Phys. Rev. Lett.* **55**, 1892.
Dullien, F. A. L., 1979, *Porous Media. Fluid Transport and Pore Structure*, Academic Press, New York.
Gray, W. G., 1975, *Chem. Eng. Sci.* **30**, 229.
Hassanizadeh, M. and Gray, W. G., 1979, *Adv. in Water Res.* **2**, 131.
Heiba, A. A., Sahimi, M., Scriven, L. E., and Davis, H. T., 1982, SPE 11015, presented at the 57th Annual Meeting of the SPE, New Orleans, 28–30 Sept. 1982.
King, P. R., 1987, *J. Phys. A* **20**, L529.
Koplik, J. and Lasseter, T. J., 1984, *Chem. Eng. Comm.* **26**, 285.
Lenormand, R., Touboul, E., and Zarcone, C., 1988, *J. Fluid Mech.* **189**, 165.
Lenormand, R., 1986a, SPE 14882.
Lenormand, R., 1986b, *Physica* **140A**, 114.
Lenormand, R., 1989, *Proc. R. Soc. London, A* **423**, 159.
Lenormand, R. and Zarcone, C., 1984, SPE 13264.
Lenormand, R. and Zarcone, C., 1985, *Phys. Rev. Lett.* **54**, 2226.
Leverett, M. C., 1941, *Trans. AIME* **142**, 152.
Levine, S. and Cutheill, D. L., 1986, *J. Canad. Petrol. Technol.* **25**, 74.
Lungren, T. S., 1972, *J. Fluid Mech.* **51**, 273.
Måløy, K. J., Feder, T., and Jøssang, T., 1985, *Phys. Rev. Lett.* **55**, 2688.
Marle, C. M., 1981, *Multiphase Flow in Porous Media*, Gulf Publishing, Houston, Texas.
Matheron, G., 1967, *Rev. de l'Institut Francais du Petrole* **3**, 443.
Miller, E. E. and Miller, R. D., 1956, *J. Appl. Phys.* **27**, 324.
Muskat, M. and Meres, M. W., 1936, *Physics* **7**, 346.
Nittmann, J., Daccord, G., and Stanley, H. E., 1985, *Nature* **314**, 141.
Pavonne, D., 1989, *Proc. IMA Conf. on the Mathematics of Oil Recovery*, Cambridge, July 1989 (to be published).
Payatakes, A. C., 1982, *Ann. Rev. Fluid Mech.* **14**, 365.
Peaceman, D. W., 1977, *Fundamentals of Numerical Reservoir Simulation*, Elsevier, Amsterdam.
Poreh, M. and Elata, C., 1966, *Israel J. Technol.* **4**, 214.
Ripley, B. D., 1981, *Spatial Statistics*, Wiley, New York, pp. 38–44.
Rubenstein, J., 1986, *J. Fluid Mech.* **170**, 379.
Scheidegger, A. E., 1954, *J. Appl. Phys.* **25**, 994.
Stokes, J. P., Weitz, D. A., Gollub, J. P., Dougherty, A., Robbins, M. O., Chaikin, P. M., and Lindsay, H. M., 1986, *Phys. Rev. Lett.* **57**, 1718.
Whitaker, S., 1966, *Chem. Eng. Sci.* **21**, 291.
Whitaker, S., 1986, *Transport in Porous Media* **1**, 3.
Wilkinson, D. and Willemsen, J. F., 1983, *J. Phys. A*, **16**, 3365.